Brain, Behavior, & Immunity - Health 28 (2023) 100599

Contents lists available at ScienceDirect

Brain, Behavior, & Immunity - Health

journal homepage: www.editorialmanager.com/bbih/default.aspx

Chronic treatment with baicalein alleviates behavioural disorders and improves cerebral blood flow via reverting metabolic abnormalities in a J20 transgenic mouse model of Alzheimer's disease

Li Zhang [a,b], Ling Rong Wong [b], Peiyan Wong [c], Wanxiang Shen [d], Shili Yang [b], Lizhen Huang [e], Yun-An Lim [f], Paul Chi-Lui Ho [a,b,g,*]

[a] Integrative Sciences and Engineering Programme, NUS Graduate School, National University of Singapore, Singapore, 117583, Singapore
[b] Department of Pharmacy, Faculty of Science, National University of Singapore, Singapore, 117543, Singapore
[c] Neuroscience Phenotyping Core, Department of Pharmacology, Yong Loo Lin School of Medicine, National University of Singapore, 117456, Singapore
[d] Department of Chemistry, Faculty of Science, National University of Singapore, Singapore, 117543, Singapore
[e] School of Biology and Biological Engineering, South China University of Technology, Guangzhou, 510006, China
[f] Department of Pharmacology, Yong Loo Lin School of Medicine, National University of Singapore, Singapore, 117600, Singapore
[g] Monash University Malaysia, School of Pharmacy, Subang Jaya, 47500, Selangor, Malaysia

ARTICLE INFO

Keywords:
Alzheimer's disease
Chronic study
Baicalein
Neurobehavioural test
Cerebral blood flow
Metabolomics

ABSTRACT

Baicalein (BE) has both antioxidant and anti-inflammatory effects. It has also been reported able to improve cerebral blood circulation in brain ischemic injury. However, its chronic efficacy and metabolomics in Alzheimer's disease (AD) remain unknown. In this study, BE at 80 mg/kg was administrated through the oral route in J20 AD transgenic mice aged from aged 4 months to aged 10 months. Metabolic- and neurobehavioural phenotyping was done before and after 6 months' treatment to evaluate the drug efficacy and the relevant mechanisms. Meanwhile, molecular docking was used to study the binding affinity of BE and poly (ADP-ribose) polymerase-1 (PARP-1) which is related to neuronal injury. The open field test showed that BE could suppress hyperactivity in J20 mice and increase the frequency of the target quadrant crossing in the Morris Water Maze test. More importantly, BE restored cerebral blood flow back to the normal level after the chronic treatment. A ^{1}H NMR-based metabolomics study showed that BE treatment could restore the tricarboxylic acid cycle in plasma. And such a treatment could suppress oxidative stress, inhibit neuroinflammation, alleviate mitochondrial dysfunction, improve neurotransmission, and restore amino homeostasis via starch and sucrose metabolism and glycolipid metabolism in the cortex and hippocampus, which could affect the behavioural and cerebral blood flow. These findings showed that BE is a potential therapeutic agent for AD.

1. Introduction

Alzheimer's disease (AD) is a complex, irreversible, and progressive neurodegenerative disorder among the elderly. Apart from amyloid beta plaques and tau tangles accumulation in the brain, AD patients also suffer from neuro-oxidative stress, neuroinflammation, impaired mitochondrial activity, disrupted neurotransmission, and aberrant lipid metabolism, which could be triggered by the abnormal accumulation of amyloid beta plaques and tau tangles (Gonzalez-Dominguez et al., 2014b; Liu et al., 2021). Meanwhile, cerebral blood flow (CBF) which accounts for the supply of oxygen and glucose in the brain has been found reduced in AD patients (de Jong et al., 2019). The oxidative stress and neuroinflammation caused by neurotoxic molecules reduce CBF, which further increases the accumulation of neurotoxic molecules in the brain (Badhwar et al., 2017; Zhang et al., 2017). Therefore, the suppression of oxidative stress and neuroinflammation could potentially alleviate AD symptoms, revert metabolic abnormalities, and restore CBF in the brain.

Our previous study revealed that baicalein (5,6,7-trihydroxyflavone, BE, Fig. 1A) had antioxidant and anti-inflammatory effects, indicating its potential in AD treatment (Zhang et al., 2020). It has been reported that BE could regulate blood flow and protect cerebral tissues from ischemic injury by inhibiting the activation of poly (ADP-ribose) polymerase-1 (PARP-1) through PI3K/AKT pathway (Huang et al., 2005; Li et al., 2020). Daily oral administration of BE at 100 mg/kg for

* Corresponding author. Department of Pharmacy, Faculty of Science, National University of Singapore, Singapore, 117543, Singapore.
E-mail address: paul.ho@nus.edu.sg (P.C.-L. Ho).

https://doi.org/10.1016/j.bbih.2023.100599
Received 26 September 2022; Received in revised form 21 January 2023; Accepted 29 January 2023
Available online 31 January 2023

Abbreviations

Acetonitrile ACN
Alzheimer's disease AD
AutoDockTools ADT
Baicalein BE
Cerebral blood flow CBF
Fold-change FC
Human Metabolome Database HDMB
Institutional Animal Care and Use Committee IACUC
Internal standard IS
Kyoto Encyclopedia of Genes and Genomes KEGG
Methanol MeOH
Morris water maze test MWM
National Advisory Committee on Laboratory Animal Research NACLAR
Nuclear magnetic resonance NMR
One-dimensional 1D
Open field test OFT
Orthogonal partial least squares discriminant analysis OPLS-DA
Partial least squares discriminant analysis PLS-DA
Peanut butter PB
Poly (ADP-ribose) polymerase-1 PARP-1
Principal component analysis PCA
Root mean square deviation RMSD
Transgenic Tg
Tricarboxylic acid cycle TCA cycle
Wildtype WT
Trimethylsilylpropanoic acid TSP
Variable importance in projection VIP

27 days in rats with occlusion of bilateral common carotid arteries attenuated cognitive impairment (He et al., 2009). Since PARP-1 activation is also involved in oxidative stress and neuroinflammation in the brain of AD patients, we hypothesize that treatment with BE could restore CBF in AD brains by inhibiting PARP-1 activation, oxidative stress, and neuroinflammation, therefore the cognitive impairment could be suppressed (Thapa et al., 2021).

It is always challenging to test the chronic treatment in transgenic

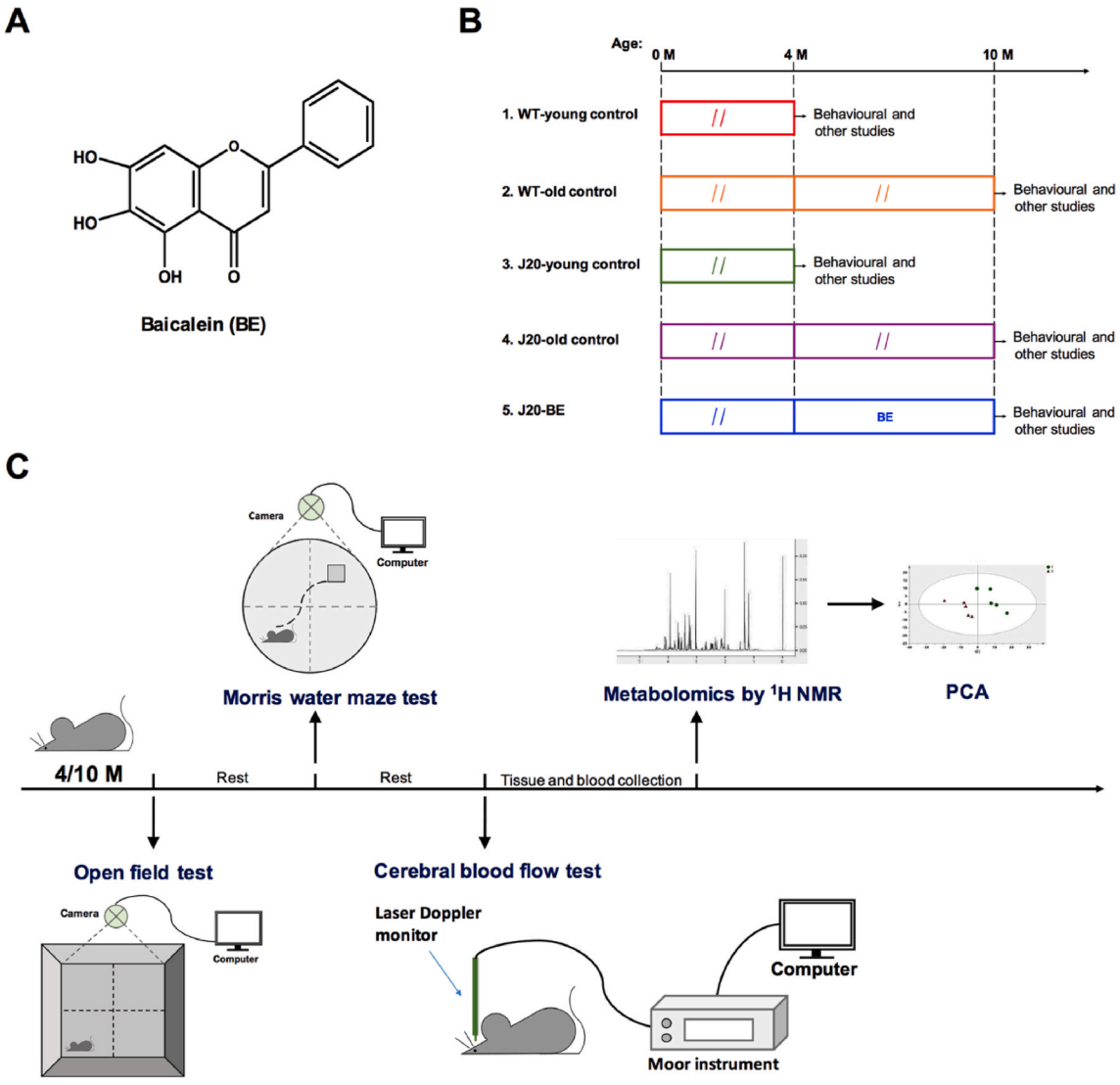

Fig. 1. The chemical structure of baicalein (A), (B) animal treatment design, and (C) behavioural (open field test) and cerebral blood flow test of WT and J20 mice after treatment in this study. n = 8 (WT-young control), 8 (WT-old control), 8 (J20-young control), 5 (J20-old control), and 5 (J20-BE) mice.

mice, but the findings of which could duly reflect the drug efficacy. Compared to the traditional forced oral gavage, the peanut butter-mixed pellets (PB) taken voluntarily by animals after training would be a much gentler route to minimise the stress response in animals, especially in multi-months' studies (Gonzales et al., 2014). Thus, the evaluation of the long-term efficiency of BE treatment in transgenic mice could be made feasible by using BE mixed PB.

To analyse the efficiency of BE, apart from the behavioural and CBF tests, metabolomics is a powerful tool to evaluate the mechanisms of action (Rong et al., 2019; Wang et al., 2014). Metabolomics could identify potential biomarkers, provide general pictures of the whole metabolites, and understand the mechanistic pathways (Wang et al., 2014). This technique could divide into targeted- and untargeted-metabolomics. The untargeted metabolomics could give an unbiased overview of alterations in metabolites of AD samples and be used for the discovery of new biomarkers and underlying mechanisms of effects (Griffiths et al., 2010). Among the techniques of metabolomics, the nuclear magnetic resonance (NMR) spectroscopy-based non--targeted metabolomic approach is non-destructive to samples, easy to reproduce, and straightforward in sample preparation (Verwaest et al., 2011). Moreover, most metabolomics studies in AD tend to focus on comparisons between healthy and diseased samples, whereas drug effect-related metabolomics studies in AD are limited, our metabolomics study of drug-treated samples could offer a deep understanding of the BE effects in the J20 AD mouse model.

In this study, we aim to evaluate the *in vivo* pharmacodynamics of BE through a 6-months' study with a J20 AD transgenic mouse model. After chronic drug treatment, behavioural tests were carried out to assess the memory and cognition capability of the J20 mice. Concurrently, the corresponding CBF levels were also measured. Finally, the metabolomics profiles of plasma and different brain parts of these mice were analysed using ^{1}H NMR to reveal the mechanism of BE from a metabolic view. Our findings through the *in vivo* study provide scientific rationales for the therapeutic application of BE in AD.

2. Materials and methods

2.1. Materials

Baicalein (BE) was purchased from Tokyo Chemical Industry Co., Ltd. (Tokyo, Japan). Deuterium oxide was purchased from Sigma-Aldrich (St Louis, MO, USA). All other reagents and solvents used were of analytical grade.

2.2. Molecular docking

To understand the potency of BE at the molecular level, the binding affinity of BE to PARP-1 protein was estimated by molecular docking with AutoDockTools 1.5.6 software (Wong et al., 2021). The crystal structure of PARP-1 protein was obtained from RCSB Protein Data Bank. The ligand, BE was prepared by Marvin sketch and the 3D confirmers with the lowest energy were obtained by using the MMFF94 force field minimization. Polar hydrogens were added to identify atom types for scoring purposes. The rotation roots and number of the rotation bonds were detected by AutoDockTools 1.5.6 software. The docking parameter of exhaustiveness was set to 100 to achieve high precision. The root mean square deviation (RMSD) value of the protein backbone and BE was calculated by web server LigRMSD, and the ligand-receptor interaction was visualized by PyMol and LigPlot+.

2.3. Animals

Male J20 mice (carrying both Swedish (K670N and M671L) and Indiana (V7171F) APP human mutations of familial Alzheimer's disease on a C57BL/6 x DBA2J background) and the wildtype (WT) littermate C57BL/6 mice were kindly provided by Professor G. S. Dawe (Department of Pharmacology, National University of Singapore, Singapore). The transgenic mice were genotyped by polymerase chain reaction with specific human APP primers. WT mice taken from the same breeding colony served as the healthy controls.

Mice were housed in cages with a maximum of 5 mice per cage under standard conditions with free access to food and water. All animal experiments were conducted in accordance with the Singapore National Advisory Committee on Laboratory Animal Research (NACLAR) guidelines and approved by the Institutional Animal Care and Use Committee (IACUC), National University of Singapore.

2.4. Experimental design

Male WT mice (n = 16) were divided into the WT-young control group (n = 8) and the WT-old control group (n = 8). Male J20 transgenic mice (n = 18) were divided into the J20-young control group (n = 8), the J20-old control group (n = 5), and the J20-BE group (n = 5, Fig. 1B). WT-young controls and J20-young controls aged 4 months old were subjected to behavioural, CBF, and metabolomics tests without any treatment served as young control groups. WT-old controls and J20-old controls were housed at the standard condition until 10 months old and served as old control. J20-BE group received a daily dose of PB pellets containing BE (80 mg/kg) starting from 4 months of age for 6 consecutive months to 10 months of age. This dose was chosen because it has been reported that oral treatment with this dose for 40 consecutive days could decrease the escape latencies and distances travelled in amyloid-β induced AD Sprague-Dawley rats in the Morris water maze test (Wei et al., 2014). When the old control and drug-treated groups reached 10 months of age, the mice were subjected to the above tests. The group sizes varied from 5 to 8 was comparable to a recent study leveraging on behavioural and metabolomics testing for their experiments (Li et al., 2021).

2.5. Preparation of drug-containing peanut butter pellets

In the chronic study, the BE-treated group was administered drug-containing peanut butter (PB, Reese's Cold Storage, Singapore) pellets prepared weekly based on the body weight of mice (Gonzales et al., 2014). 100 mg PB was used as a vehicle for the daily dose of BE. The daily required amount of BE powder was added to melted PB and mixed homogenously to form pellets and stored at −20 °C. Each formed pellet weighed 100 ± 5 mg. The drug amounts in the pellets (BE-PB) were tested by HPLC. Prior to the initiation of drug treatment, PB-only pellets were placed into the animal cages once a day for 7 continuous days to allow the mice to become acclimatised to voluntary feeding on the PB pellets. At the end of habituation, each mouse could finish one PB pellet within 10 min.

2.6. Drug administration

The J20 mice aged 4 months were administrated with BE-PB once daily at 14:00 (±30 min) h for consecutive 6 months. One BE-PB was placed in a clean cage with bedding. Then one mouse was transferred into the clean cage and was given 10 min to find the pellet, grasped the pellet with its forepaws, and fully consumed the pellet. Finally, this mouse returned to its home cage. Then the treatment was followed by another mouse. The whole process was finished within 30 min.

2.7. Behavioural studies

All mice were subjected to behavioural tests including the open field test (OFT) and Morris water maze test (MWM) when reaching 4 and/or 10 months of age with/without drug treatment (Fig. 1C). Only one test was conducted on each test day. The mice had multiple days of rest between the two experiments to minimise carryover effects. All behavioural tests were performed in specialised experimental rooms to avoid

environmental or physical stress on mice. Before initializing each test, the mice were allowed at least 30 min of habituation period in the experimental room with free access to food and water.

2.7.1. Open field test

Locomotor activity was recorded using a square open field (40 × 40 cm) in a plexiglass cage in the OFT test. The mice were transferred into the test cage and allowed to explore freely for 1 h without disturbance. Locomotor activity was recorded automatically with a video camera fixed above the cage. The mice were returned to their respective home cages after the test. The plexiglass cage was carefully cleaned before the next run. The recorded data were analysed for the total distance travelled using Topscan software (CleverSys Inc, VA, USA).

2.7.2. Morris water maze test

The MWM test was conducted in a circular pool with a diameter of 1.2 m. The pool water temperature was kept at 24–26 °C throughout the experiment. The water inside the pool was made murky with non-toxic white paint. A circular platform with a diameter of 9 cm was hidden 1.5 cm below the water surface at a fixed position. The pool area was divided into 4 equal quadrants. The target quadrant hidden platform was in the centre of the southeast quadrant. The mice were given 60 s to explore in each training trial. If the mice could not find the platform within 60 s, they were guided to the platform and allowed to remain there for 10 s. The mice were trained 4 times a day for 5 consecutive days. The time spent from the start point to reach the platform was recorded as latency to the target platform to obtain a learning curve. During the probe trial, the platform was removed and the mice were given 60 s in the pool. The time recording was started once the mice were placed into the pool. The latency to the target platform, the number of quadrant visits, and the average swimming speed were recorded in the probe test. After tests, the mice were dried with a towel and returned to their home cages. All MWM trials were video-recorded and analysed using the Topscan software.

2.8. Cerebral blood flow test

CBF measurements were performed on the mice with a Laser Doppler Monitor (moor VMS-LDF1, Moor Instruments Inc., Devon, UK) after behavioural tests (Poinsatte et al., 2015; Rajasekar et al., 2017). At least 5 mice in each group were subjected to CBF measurements. Each mouse was first anesthetized using 4% isofluorane mixed with 1–2 L/min of oxygen. Next, the mouse's head was fixed using a stereotactic apparatus in the prone position. Anesthesia was maintained using 2% isofluorane mixed with 1–2 L/min of oxygen. A midline sagittal incision was made using surgical scissors. After the skin underneath was carefully removed to each side, the bone over the cortex was thinned using a small hand drill until only a small translucent sheet of the bone remained. The laser Doppler probe was positioned at 5.5 mm lateral-right, 1 mm caudal from the bregma, and 5 mm above the head. The probe was fixed in a vertical position with a clamp. The blood flow was recorded until getting a stable flux and the average flux during this stable period was regarded as the baseline CBF of the mouse. The entire process for each mouse took around 40 min.

2.9. Tissue sample collection and preparation

After the CBF measurement, the mouse was sacrificed by CO_2 euthanasia. Blood samples were collected immediately via cardiac puncture and transferred into Eppendorf tubes containing 3 μL heparin. The collected blood samples were centrifuged at 4000 g for 5 min at room temperature to get plasma (Zhang et al., 2020). The plasma was collected and cooled down in an ice bath. Then the mice were perfused with saline to remove the blood in the organs. The brains were carefully isolated and washed with saline to remove the surface blood. Plasma and different major parts of the brain including the cerebellum, midbrain, cortex, and hippocampus were collected and stored at −80 °C for future analysis.

To extract metabolites for NMR analysis, the frozen plasma was allowed to gradually thaw in an ice bath. For brain samples, 20 mg of various brain tissues were weighed separately. 200 μL ice cold water was added and the mixture was homogenized for 1 min using a bead homogenizer (Bullet Blender 24 Gold, Next Advance, NY, USA). 200 μL homogenate was transferred to another clean tube. Then 200 μL cold ACN and 200 μL cold MeOH were added into the plasma/brain homogenate and vortexed for 5 min. The mixture was centrifuged at 14,000 g for 20 min at 4 °C. 550 μL of supernatant containing the extracted polar metabolites was collected and dried by blowing nitrogen gas at room temperature. The dried residue was kept at −80 °C until future analysis.

2.10. ^1H NMR spectroscopy

Each dried residue was re-suspended with 600 μL deuterium oxide buffer (pH 7.4) containing 50 mM sodium phosphate and 0.1 mM trimethylsilylpropanoic acid (TSP) as the internal standard (IS). The mixture was vortexed for 5 min and centrifuged at 14,000 g for 10 min at 20 °C. 550 μL supernatant was transferred into an 800 MHz NMR tube with a 5 mm diameter for analysis.

The nuclear magnetic resonance (NMR) spectroscopy was performed using a Bruker AVANCE 800 MHz system equipped with an inverse triple-resonance cryoprobe (5 mm diameter). The ^{1}H NMR spectra were acquired at 298 K. A Carr-Purcell-Meiboom-Gill pulse sequence with pre-saturation was applied as a T_2 filter to remove the signals of macromolecules and water. All one-dimensional (1D) spectra were obtained through 512 transients collected into 64 K data points with a spectral width of 12,820 Hz and an acquisition time of 2.56 s. The 1D NMR spectra were manually phased. The baseline of each spectrum was corrected and shifted to 0 ppm based on the TSP reference using TopSpin software 2.1 (Bruker Biospin, UK). The acquired ^{1}H NMR raw data were first imported into Chenomx NMR Suite software 7.1 (Chenomx Inc., Canada), following which the peaks from 0.04 to 10.00 p.m. were manually binned into 0.04 ppm wide buckets. The water region from 4.68 to 4.88 ppm was excluded. The MeOH signal from 3.32 to 3.36 ppm was also excluded. All binned data were normalised according to the total binned area in each data file.

2.11. Multivariate data analysis

The binned data from different matrices were subjected to multivariate data analysis with SIMCA-P 13.0 software (Umetrics, Umeå, Sweden). Data were Pareto-scaled prior to principal component analysis (PCA) to give a direct observation of cluster trend. Then the data were subjected to partial least squares discriminant analysis (PLS-DA) to promote the separation between two or more groups and build a discriminant model. The model was evaluated by the parameters including R^2(Y) and Q^2(cum) obtained through 100 observation-dependent randomised permutation tests. Subsequently, the data were analysed by orthogonal partial least squares discriminant analysis (OPLS-DA) to identify the metabolites that had significant contributions to the differences between the two groups. Variables with variable importance in projection (VIP) value > 1.0 and p value < 0.05 of CV-ANOVA were selected to identify the potential discriminant metabolites.

2.12. Potential discriminant metabolite identification

The potential discriminant metabolites were identified with reference to the chemical shifts of pure compounds available from the databases of Chenomx NMR Suite software 7.1 (Chenomx Inc., Canada) and Human Metabolome Database (HMDB, https://hmdb.ca). The concentrations of the specific metabolites were calculated by comparing the area of the signals of metabolites to that of TSP. The fold-change (FC)

value of each discriminant metabolite was calculated using the following equation:

$$FC = \frac{I_A}{I_{WTold}}$$

I_A represents the average concentration of the specific metabolite in group A while I_{WTold} represents the average concentration of the specific metabolite in the WT-old control group.

2.13. Metabolic pathway analysis

Metabolic pathway analysis was carried out using Metaboanalyst 5.0 software, a web-based analysis tool (https://www.metaboanalyst.ca). This platform supports quantitative metabolomics data analysis, including ~1600 metabolic pathways for different species based on the databases of the Kyoto Encyclopedia of Genes and Genomes (KEGG) and HMDB.

2.14. Data and statistical analysis

All results are reported as mean ± SD unless otherwise indicated. Statistical analyses were performed by two-way ANOVA and Tukey's test for comparison among multiple groups and unpaired student's *t-test* for comparison between two groups. The significant difference was defined as $p < 0.05$. All statistical analyses and graphs were plotted using GraphPad Prism 7 (GraphPad Software, San Diego, CA, USA).

3. Results

3.1. Molecular docking

According to Fig. 2, the docking results showed the binding affinity of PARP-1-BE was −8.4 kcal/mol. The root-mean-square deviation (RMSD) value of PARP-1-BE was 2.3 Å. Gly863 and Tyr896 were the major residues forming the hydrogen bonds between PAPR-1 and BE. The molecular docking results showed the binding affinity of BE to PARP-1 protein.

3.2. Open field test

The body weight of mice was weighed before the OFT test. In Fig. S1, the weight of mice in the J20-old control group and J20-BE group did not show a significant difference, indicating the PB formulations did not show any obvious adverse effects on the mice. The change in body weight of WT young and old control mice was not significant, which may be due to the small number of mice in this study.

OFT was used to evaluate the locomotor performance of mice by comparing the total travelled distance (Ma et al., 2020). The total travelled distance in the J20-young control group was 1.88-fold as that of the WT-young group, indicating transgenic mice significantly moved more (Fig. 3A, $p < 0.05$). This observed trend was consistent with a previous report (Sun et al., 2008). Meanwhile, the J20 old control mice were still more hyperactive than the respective WT young and old control mice, though no significant difference was observed. After chronic treatment with BE for 6 months, the total travelled distance decreased to 68.75% of the J20-old control group ($p > 0.05$), bringing the mean value in between that of the WT young and old control mice. Therefore, BE treatment could normalize the locomotor activity in J20 mice.

3.3. Morris water maze test

MWM test was performed to evaluate the spatial acquisition of mice. In Fig. 3B depicting the learning curves, there was no difference among these groups on the 1st training day. After 5 days of training, the average latency to the platform in the WT-old control group was only 26.43% as that of the J20-old group ($p < 0.05$). Other groups did not show significant differences. On the test day, the latency to platform of all groups was around 40 s, which did not display obvious differences, including the drug-treated mice compared to the J20-old controls (Fig. 3C). However, J20-old control mice showed a lower frequency of target quadrant crossing than the WT-old control mice, indicating memory deficit in J20 mice aged 10 months (Fig. 3D, $p < 0.05$). The target quadrant crossing frequency of drug-treated J20 groups was higher than the J20-old control group and comparable with the WT-old control group, suggesting BE could improve cognition in J20 mice. In addition, the average swimming speed was also analysed to evaluate the motor function of mice (Saffari et al., 2020). In Fig. 3E, the mean speed of J20-old control mice was 56.85% as that of the WT-old control group. After treatment with BE, the swimming speed of J20 mice increased to a level comparable to the WT-old control group. Thus, long-term treatment helps to normalize the motor activity of AD mice.

3.4. Cerebral blood flow test

A laser Doppler Monitor was used to measure the CBF in the brain as the probe is sensitive to blood flow (Liu et al., 2018). The average CBF flux in the WT-young control was comparable with the WT-old control group (Fig. 3F). Meanwhile, the J20-young control mice did not show obvious CBF reduction compared to the WT-young control mice. However, the CBF of the J20-old control group was only 55.94% of the WT-old control group ($p > 0.05$). A similar trend was also reported in another study (Lin et al., 2013). After chronic treatment with BE, CBF increased in the J20-BE group to a level comparable to the WT-old

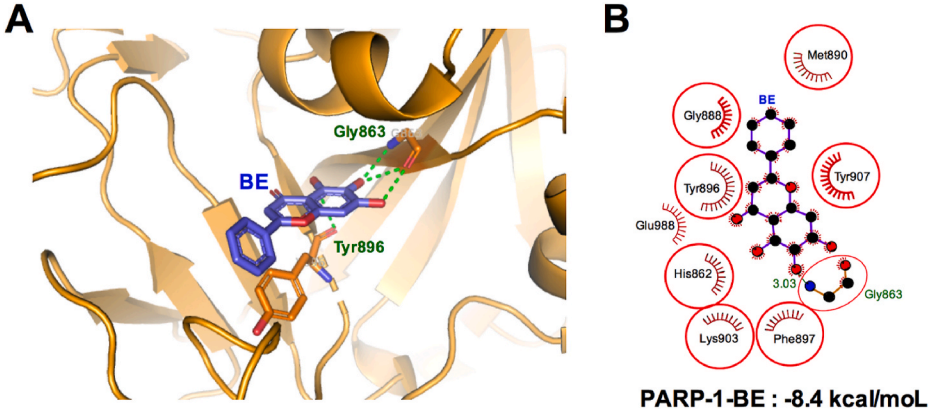

Fig. 2. 3-Dimensional visualization by PyMol software (A) and 2-Dimensional visualization by LigPlot + software (B) molecular docking study PARP-1 protein with Baicalein (BE). The red circles indicate the same residues in the interaction.

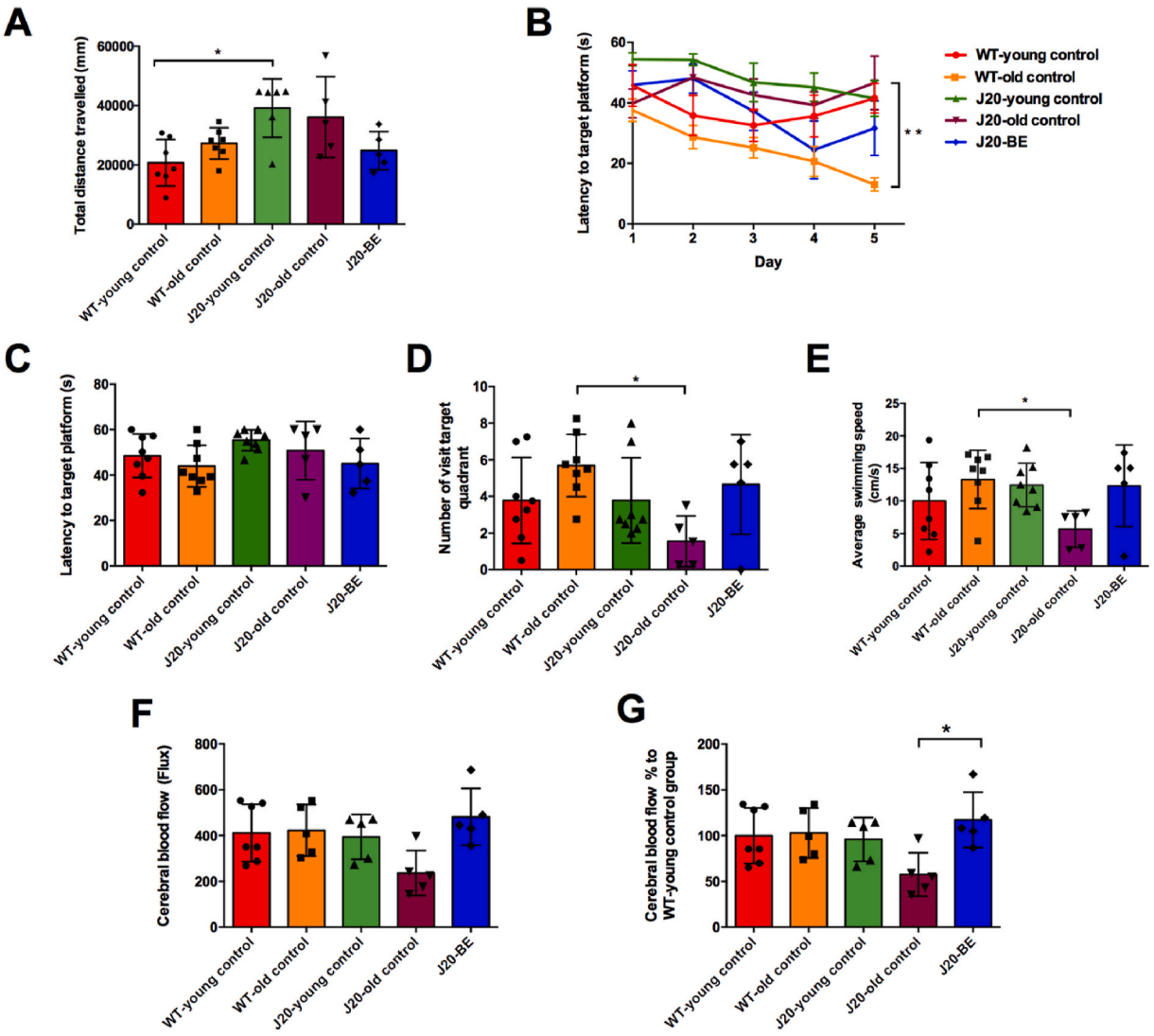

Fig. 3. The behavioural and cerebral blood flow tests of mice after chronic treatment. (A) The total distance travelled the respective groups in the open field test. (B–E) The Morris water maze test in J20 mice and WT mice of the respective groups. (B) The average latencies to the target platform across the training 5 days. (C) The average latencies to the target platform of the probe trial. (D) The number of visit quadrant within 60 s in the probe trial. (E) The average swimming speed of the mice within 60 s in the probe trial. (F) The cerebral blood flow flux via laser Doppler cytometry test in J20 mice and WT mice of the respective groups. (G) The comparison of cerebral blood flow of the WT-young group with other groups. Data are reported as mean ± SD (n = 5–8). * indicates $p < 0.05$ between the two groups. ** indicates $p < 0.01$ between the J20 old group and the WT old group.

control group and showed a significant difference compared to the J20-old control group (Fig. 3G, $p < 0.05$). Therefore, chronic administration of BE normalised the impaired CBF in the brains of old AD mice.

3.5. Comparative metabolome analysis of plasma samples

PCA method was applied to generate an overall picture of metabolic data, which can directly display the clusters in different groups (Peng et al., 2014). The metabolites of plasma samples in WT young and old control did not show any age-related differences, which was consistent with a previous study that showed no obvious difference in metabolites of plasma samples between the male C57BL/6J mice aged 15 weeks and 45 weeks through NMR tests (Varshavi et al., 2018). The PCA result for plasma samples of WT control and J20 control mice did not show obvious clustering trends on the scores plot, indicating no significant changes in metabolic profiles in the plasma of these two groups (Fig. 4A). Neither the plasma samples of the J20-old control group nor the WT-old control group shows a clear cluster separation, suggesting the metabolomic changes in the plasma of old transgenic mice were limited. However, after the long-term treatment, the plasma samples of the J20-BE group showed a clear cluster separation from the J20 old control group, indicating that BE treatment could cause a metabolic change that was reflected in the plasma metabolic profiles (Fig. 4A&S2B).

Compared to the WT control mice, the identified metabolites of plasma samples in the J20 control mice of the same age did not show obvious changes from PLS-DA and OPLS-DA models, which was consistent with PCA results (Fig. 4B). The levels of adenine and succinate in the J20-BE group decreased to comparable levels with the WT-old control group. In contrast, the levels of alanine, citrate, lactate, and tryptophan in the J20-BE group showed some changes compared with other groups but no significant difference was observed. Based on the identified metabolites, metabolic pathway analysis was performed using Metaboanalyst 5.0 software. Fig. 4C and D shows that the altered pathway depicted in the plasma of the J20-BE group was related to the tricarboxylic acid cycle (TCA cycle) on energy production. Thus, BE treatment could restore energy production in J20 old mice.

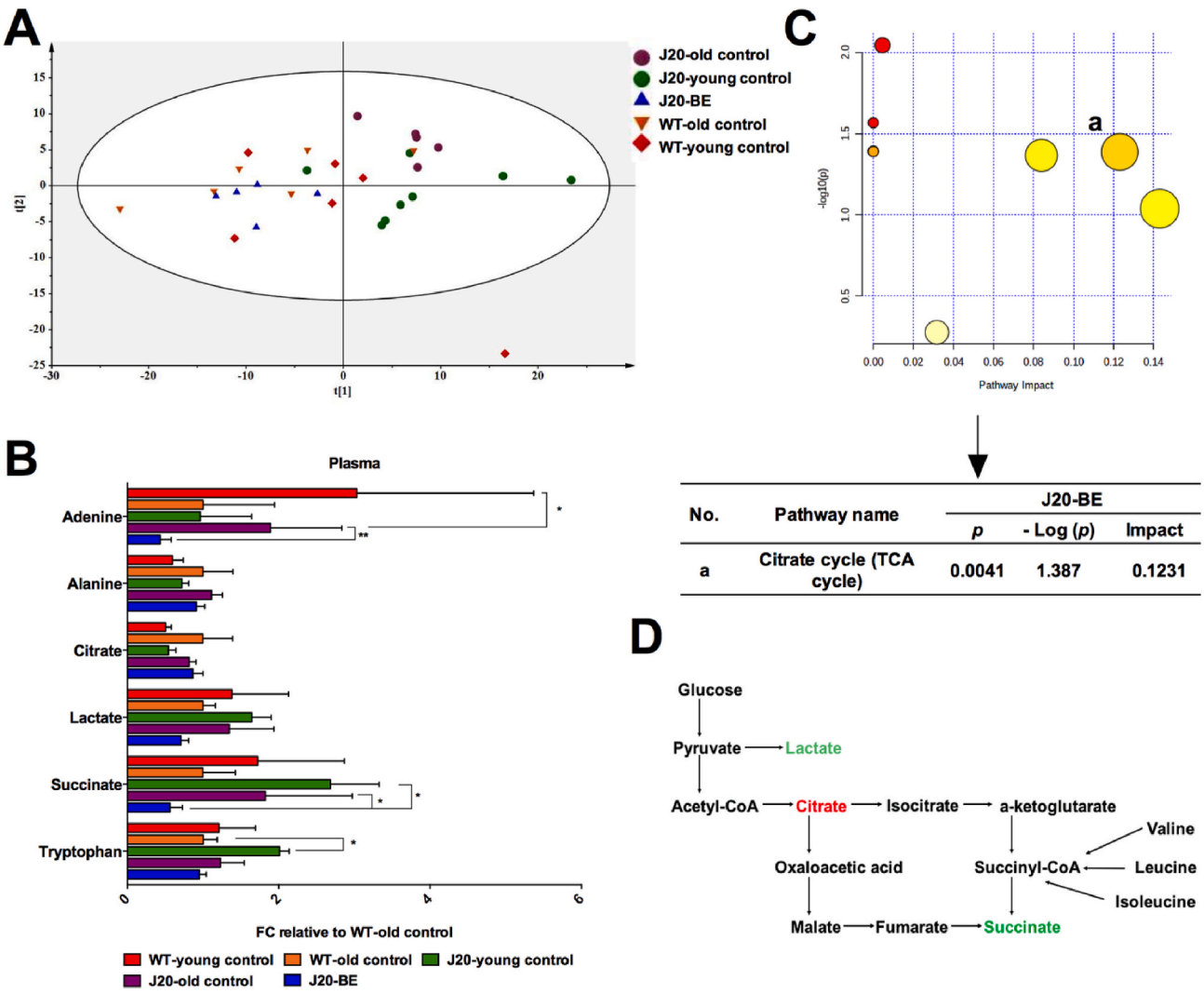

Fig. 4. Comparative metabolome analysis of plasma samples of different groups. (A) PCA score plots of plasma metabolic profiles from different groups. Each symbol represents one ^{1}H NMR spectra from different groups. (B) The relative fold of identified metabolite biomarkers in plasma samples of the respective groups compared with the WT old group. Data are reported as mean ± SD (n = 5–8). * indicates $p < 0.05$, ** indicates $p < 0.01$, and *** indicates $p < 0.001$ between the compared two groups. (C) The metabolism pathway analysis overview in plasma samples from J20 mice after chronic treatment of BE. (D) The most typical altered biosynthetic and metabolomics pathway in plasma samples from J20 mice after chronic treatment of BE. Green represents the down-regulated contents and red represents the up-regulated contents.

3.6. Comparative metabolome analysis of cortical tissues

PCA for cortex metabolic profiles of WT- and J20-control groups did not show any obvious cluster separations (Fig. 5A&S3A). Thus, the changes in metabolic profiles of cortical tissues from J20 transgenic mice were not obvious compared to WT mice. However, the cortex metabolic profiles of J20 control mice and BE-treated mice displayed a clear separation, indicating the metabolic alterations in the cortex after BE treatment (Fig. S3B).

12 potential discriminant metabolites were generated in cortical tissues (Fig. 5B). The levels of adenine, carnitine, and glycerol were lower in the WT old than WT young control group. The other 9 metabolites did not show any significant difference, suggesting that these metabolites were not age-dependent. The levels of adenine, carnitine, and glycerol were significantly increased in the J20-old group compared with the WT-old group. These changes showed there were still abnormalities in the cortex of J20 old mice although the PCA study didn't show clear cluster separation. The metabolites that displayed a significant reduction ($p < 0.05$) in the J20-BE group than the J20-old control group are: adenine, carnitine, γ-aminobutyrate (GABA), glycerol, inosine, 3-methylxanthine, and phenylalanine. The levels of isoleucine, leucine, phosphorylcholine, tyrosine, and valine showed a reduction trend after treatment with BE compared to the J20-old control group but no significant differences. The altered metabolites suggest that chronic treatment with BE affected the metabolic profiles in the cortical tissues.

The metabolic pathways affected by BE treatment compared to the J20-old control group are, phenylalanine, tyrosine and tryptophan biosynthesis; phenylalanine metabolism; glycolipid metabolism; and tyrosine metabolism (Fig. 5C). The typical pathway affected after treatment with BE was glycerolipid metabolism based on the down-regulation of glycerol after treatment (Fig. 5D). Since abnormal glycerolipid metabolism has been observed in AD, restoration of glycerolipid metabolism through BE could be beneficial to the brain with metabolic dysfunction in AD (Gonzalez-Dominguez et al., 2015e).

3.7. Comparative metabolome analysis of hippocampal tissues

Similar to the cortex metabolic profiles, the PCA of the hippocampus metabolic profiles of the WT control mice and J20 control mice did not show any obvious cluster separations while there is a clear separation

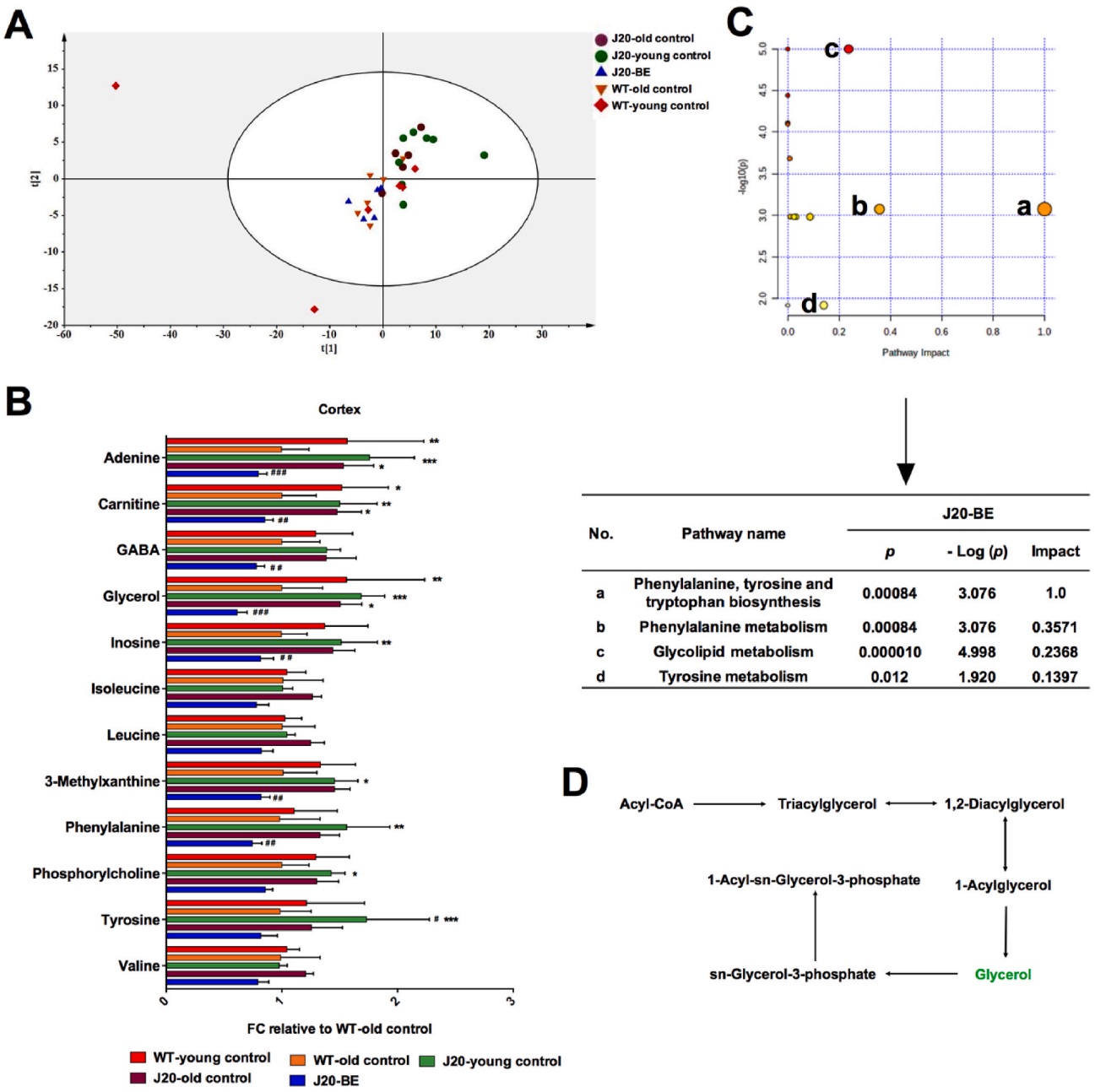

No.	Pathway name	J20-BE		
		p	- Log (*p*)	Impact
a	Phenylalanine, tyrosine and tryptophan biosynthesis	0.00084	3.076	1.0
b	Phenylalanine metabolism	0.00084	3.076	0.3571
c	Glycolipid metabolism	0.000010	4.998	0.2368
d	Tyrosine metabolism	0.012	1.920	0.1397

Fig. 5. Comparative metabolome analysis of cortex samples in different groups. (A) PCA score plots of cortex metabolic profiles from different groups. Each symbol represents one ^{1}H NMR spectra from different groups. (B). The relative fold of identified metabolite biomarkers in cortex samples of the respective groups compared with the WT old group. Data are reported as mean ± SD (n = 5–8). * indicates $p < 0.05$, ** indicates $p < 0.01$, and *** indicates $p < 0.001$ compared with WT-old control group. # indicates $p < 0.05$, # # indicates $p < 0.01$, and # # # indicates $p < 0.001$ compared with J20-old control group. (C) The metabolism pathway analysis overview in cortex samples from J20 mice after chronic treatment of BE. (D) The most typical altered biosynthetic and metabolomics pathway in cortex samples from J20 mice after chronic treatment of BE. Green represents the down-regulated contents.

between the J20 control mice and J20 BE-treated mice, indicating the metabolic alterations in their hippocampus after chronic treatment with BE (Fig. 6A&S4). 9 potential discriminant metabolites (Fig. 6B) that contributed to separations in hippocampus metabolic profiles among the groups were generated. The level of glycerol in WT old mice was lower than in young control mice, indicating an age-associated change. The level of glucose-6-phosphate was significantly upregulated in the J20 old control in contrast to the WT old-control group. Other metabolites such as adenine, glycerol, isoleucine, leucine, 3-methylxanthine, phenylalanine, tyrosine, and valine showed higher expressions in the J20-old control group than the WT-old control group, albeit no significant differences were found. These changes in metabolites' levels in the hippocampus indicated the abnormalities in the J20 old control group despite the unseparated clusters in PCA results (Fig. S4A). After the long-term treatment with BE, the levels of adenine, glucose-6-phosphate, glycerol, isoleucine, and phenylalanine in the J20-BE group were significantly lower than the J20-old control group but comparable to those of the WT-old control group. The level of glucose-6-phosphate in the J20-BE group was even lower than that of the WT-old control group. The levels of leucine, 3-methylxanthine, tyrosine, and valine in the J20 BE-treated mice showed a downregulation trend. Therefore, similar to cortical tissues, the treatment effects were obvious in the hippocampal tissues.

The affected pathways in the hippocampus are depicted in Fig. 6C.

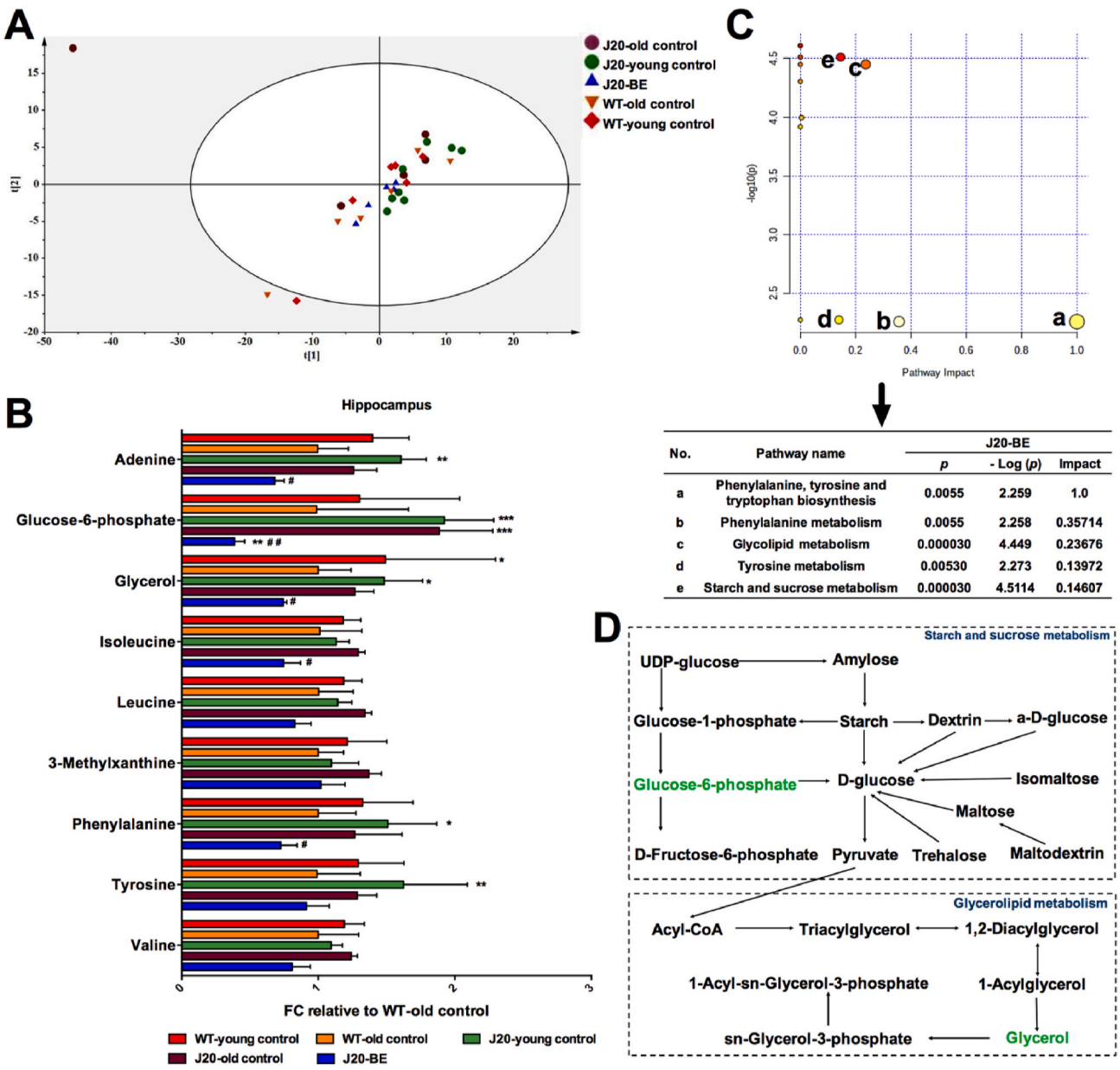

No.	Pathway name	J20-BE		
		p	- Log (*p*)	Impact
a	Phenylalanine, tyrosine and tryptophan biosynthesis	0.0055	2.259	1.0
b	Phenylalanine metabolism	0.0055	2.258	0.35714
c	Glycolipid metabolism	0.000030	4.449	0.23676
d	Tyrosine metabolism	0.00530	2.273	0.13972
e	Starch and sucrose metabolism	0.000030	4.5114	0.14607

Fig. 6. Comparative metabolome analysis of hippocampus samples in different groups. (A) PCA score plots of hippocampus metabolic profiles from different groups. Each symbol represents one ^{1}H NMR spectra from different groups. (B). The relative fold of identified metabolite biomarkers in hippocampus samples of the respective groups compared with the WT old group. Data are reported as mean ± SD (n = 5–8). * indicates $p < 0.05$, ** indicates $p < 0.01$, and *** indicates $p < 0.001$ compared with WT-old control group. # indicates $p < 0.05$, # # indicates $p < 0.01$, and # # # indicates $p < 0.001$ compared with J20-old control group. (C) The metabolism pathway analysis overview in hippocampus samples from J20 mice after chronic treatment of BE. (D) The most typical altered biosynthetic and metabolomics pathway in hippocampus samples from J20 mice after chronic treatment of BE. Green represents the down-regulated contents.

Compared to the J20-old control group, 5 metabolic pathways were changed after chronic treatment with BE, including phenylalanine, tyrosine and tryptophan biosynthesis; phenylalanine metabolism; glycolipid metabolism; tyrosine metabolism; and starch and sucrose metabolism. The most prominent pathway that was affected is starch and sucrose metabolism (Fig. 6D).

4. Discussion

In this study, the chronic treatment of BE with J20 mice for 6 months was carried out to evaluate its long-term effects in AD. Our results indicated that BE could suppress the cognitive deficits as indicated in behavioural tests, restore CBF in the brain to the normal level, and revert the metabolomic abnormalities in plasma and brain of J20 mice through ^{1}H NMR tests. These findings gave a deeper understanding of the activities of BE in the treatment of AD.

The reactive oxygen/nitrogen species in the brain of AD patients could trigger DNA damage by free radicals. Then the enzymatic activity of PARP-1 could be activated by DNA damage, which could catalyze the reaction of poly (ADP-ribose) polymers and the depletion of NAD^{+}. Finally, the persistent NAD^{+} depletion could cause loss of energy, resulting in further increased oxidative stress, neuroinflammation, mitochondrial dysfunction, and neuronal death the in brain (Martire et al., 2015). Thus, BE could be a potential therapeutic for AD because of its inhibition effect on PARP-1 hyperactivity and reactive oxygen species production, which is beneficial to the recovery of neuronal normal functions.

Unlike the models generated by the induction of compounds like Aß

and scopolamine (Aghajanzadeh et al., 2020; Liu et al., 2013), the J20 mouse model could illustrate the dynamic progression of AD. The drug administration started at 4 months of age because J20 mice started showing symptoms of AD at such an age (Hong et al., 2016). J20 male mice were used in this study, as the male mice showed more obvious cognitive deficits than J20 female mice at a young age of 3 months (Quartey et al., 2019). The PB formulations taken voluntarily by animals would be a much gentler approach compared to forced oral gavage. Since chronic treatment with PB vehicle did not cause any obvious effects in Tg2576 mice in our previous study (Wong et al., 2020), a PB vehicle group was not included in this study.

In the behavioural tests, the reduced hyperactivity in AD mice treated with BE observed in the OFT test indicated these treatments were beneficial to locomotor activity normalization (Walker et al., 2011). The differences observed in the number of quadrant visits in the MWM test were caused by differences in spatial memory and swimming speed in the J20 old mice and drug-treated J20 mice. Thus, long-term treatment with BE helped improve cognition and motor activity in AD mice (Fig. 3).

A previous study showed BE could decrease the cerebral infarct volume in rats with artificial middle cerebral artery occlusion at the dose of 100 mg/kg for 7 days (Li et al., 2020). However, the effect of BE on CBF of AD mouse models is still unknown. The average CBF in C57BL/6 (wildtype) mice aged 18 months was reported to be about 20% lower than the normal level (Hecht et al., 2012). Our results did not reveal CBF reduction in WT-old control mice, which may be due to the relatively younger age (Fig. 3F&G). The antioxidant effect of BE could protect blood vessels from oxidative damage. Its inhibition effect on the intracellular concentration of Ca^{2+} resulted in vasorelaxation and reduced blood pressure (Huang et al., 2005). Both effects could regulate the CBF. As the main energy source, the delivery of glucose is impaired when CBF reduces, which could significantly affect the energy homeostasis in the brain of Alzheimer's patients. The restoration of CBF via BE could improve the energy supplement in AD patients.

Metabolomics analyses of plasma (Fig. 4&S2) and 4 major brain regions implicated in AD namely, the cortex (Fig. 5&S3), hippocampus (Fig. 6&S4), midbrain (Fig. S5&S6), and cerebellum (Fig. S7&S8) could generate useful mechanic findings that complement existing understanding of the AD pathophysiology in the J20 mice and corresponding drug treatment effects. The cortex and hippocampus are the two most affected brain regions in AD patients, which are responsible for cognitive function (Salek et al., 2010), the metabolomic study of these two brain parts were displayed in the main context. The metabolomics changes of the midbrain and cerebellum could be seen in supplementary studies.

Carnitine is related to fatty acid transportation to mitochondria and participated in energy production (Trushina et al., 2013). Carnitine also possesses an antioxidant effect. The level of carnitine was found to be elevated in response to oxidative stress in the brain (Pena-Bautista et al., 2019). Upregulation of glucose-6-phosphate in the hippocampus of the J20-old control group also indicated oxidative stress and energy impairment (Martins et al., 1986). After drug treatment, carnitine level in the cortex and glucose-6-phosphate level in the hippocampus of J20 mice downregulated to levels comparable to the WT-old control group, indicating oxidative stress was circumvented in these tissues caused by BE (Figs. 5 and 6).

Oxidative stress is one early feature of AD, which could cause mitochondrial dysfunction. The mitochondrial activity after treatment with BE was also explored. The levels of citrate, lactate, and succinate showed an upregulation trend in the plasma of J20 old control mice, indicating energy supply impairment (Gonzalez-Dominguez et al., 2015a; Tsuruoka et al., 2013). The upregulation of adenine in plasma (Fig. 4), cortex (Fig. 5), hippocampus (Fig. 6), and midbrain (Fig. S5) samples in the J20-old control mice indicated mitochondrial toxicity in the brain (Trushina and Mielke, 2014). 3-methylxanthine was upregulated in the cortex, hippocampus, and midbrain of J20 old mice as well. It is reported that xanthine was upregulated in the brain of AD patients (Paglia et al., 2016). Since 3-methylxanthine is a derivative of xanthine, both could possess similar activities, and are purine metabolites correlating to the brain's energy state (Ibanez et al., 2013; Zhang et al., 2015). After drug treatment with BE, these metabolites in plasma and specific brain regions downregulated to levels comparable to the WT-old control group. Therefore, the mitochondrial activities in plasma, cortex, hippocampus, and midbrain were normalised after chronic treatment with BE, which is beneficial to the energy supply in the plasma and brain of AD patients.

In addition, mitochondrial function is also essential to the early stage of transmission (Guo et al., 2017). Mitochondrial dysfunction may affect neuron transmission. The increased production of phosphorylcholine could lead to reduced production of acetylcholine, which is a key neurotransmitter (Craig et al., 2011). Hence, the higher level of phosphorylcholine detected in the cortex of the J20-old control group may be related to impaired neurotransmission although the differences were not statically significant (Fig. 5). Our results showed the downregulation of phosphorylcholine after the administration of BE. Therefore, the impaired neurotransmission in the cortex could be alleviated with the chronic long-term treatment with BE.

Due to the weak antioxidant ability in the brain, oxidative stress also affects the level of fatty acid in phospholipids (Gonzalez-Dominguez et al., 2014a). The abnormal metabolism of fatty acids in AD patients could lead to the accumulation of free fatty acids in the brain, which is associated with membrane lipids degradation (Gonzalez-Dominguez et al., 2015d). Glycerol is the final product of the degradation process (Gonzalez-Dominguez et al., 2014b). The upregulated glycerol in the cortex (Fig. 5), hippocampus (Fig. 6), midbrain (Fig. S5), and cerebellum (Fig. S7) of J20-old control mice indicated the abnormal metabolism of fatty acid. After long-term treatment with BE, the glycerol level was downregulated in these four brain regions of J20 mice, suggesting a reversion of the abnormal fatty acid metabolism in the brain.

Neuroinflammation is another characteristic of the brain of AD patients. GABA is an inhibitory neurotransmitter and was reported to be downregulated in the cortex of AD mice in another study (Lalande et al., 2014). However, another study indicated GABA upregulation was related to the activation of astrocytes linked to neuroinflammation (Oksanen et al., 2019). Thus, the downregulation of GABA levels in our study suggested possible inhibition of neuroinflammation in the cortex after treatment. Phenylalanine was related to immune activation in AD which can enhance the oxidative stress of astrocytes (Wissmann et al., 2013; Zhou et al., 2021). The level of phenylalanine showed an upregulated trend in the cortex and hippocampus, and midbrain samples of the J20-old control group (Figs. 5 and 6&S5). After the chronic treatment, the level of phenylalanine in these tissues downregulated to a level comparable to the WT-old control group, demonstrating that BE could reduce neuroinflammation.

The levels of other amino acids including alanine and tryptophan in plasma; inosine in the cortex; isoleucine, leucine, tyrosine, and valine in the cortex, hippocampus, and midbrain (Figs. 4–6&S5); tyrosine in the cerebellum (Fig. S7) were altered in this study although not all changes of these metabolites show significant changes. The upregulation of alanine in plasma samples of the J20 old control group (Fig. 4) was also observed in another study (Santos et al., 2020). In contrast, the metabolism of tryptophan is complicated and the direction of change in tryptophan level in plasma varied in different studies (Gong et al., 2015). In this study, the level of tryptophan in plasma samples of the J20-BE group shows a decreasing trend compared to the J20-old control group. The upregulated inosine in J20-old control mice was linked to nucleotide degradation in the brain (Gonzalez-Dominguez et al., 2015b). Tyrosine is the precursor of catecholamine including dopamine. The change in tyrosine level suggests a disturbance of neurotransmission in the brain as well (Gonzalez-Dominguez et al., 2015c). After chronic treatment with BE, the levels of alanine and tryptophan in plasma (Fig. 4); inosine in the cortex (Fig. 5); isoleucine, leucine, tyrosine, and valine in the cortex, hippocampus, and midbrain (Figs. 5 and 6&S5); and

tyrosine in the cerebellum (Fig. S7) were restored to levels comparable to the WT-old control group, indicating that amino acid homeostasis in the plasma and brain was restored after drug treatment.

Collectively, the above results suggested the long-term treatment of BE could restore the TCA cycle in plasma and alter the metabolomics abnormalities in the brain of J20 mice. BE could amend mitochondrial dysfunction, oxidative stress, fatty acid metabolism, neurotransmission, neuroinflammation, and amino acid homeostasis in the cortex and hippocampus due to its antioxidant and anti-inflammatory ability. The main affected pathways are starch and sucrose metabolism, and glycolipid metabolism. Since the cortex and hippocampus are the key regions responsible for memory and cognition, the chronic treatment of BE could alter the abnormalities in the brain regions of AD patients. However, due to the limited amounts of tissues available in this study, the histology of Aß depositions, PARP-1 activity, and *in vivo* neuroinflammation in the brain tissues of WT, J20, and BE-treated J20 mice could not be carried out to evaluate the effects of BE in the *in vivo* studies. To get a deeper understanding of the mechanisms of actions of BE in AD, another batch of animals could be added to test for these *in vivo* effects in the future studies.

5. Conclusion

In summary, the long-term treatment with BE at a dose of 80 mg/kg for 6 months was beneficial to AD transgenic mice. BE could inhibit hyperactivity, improve spatial learning ability, and restore CBF in J20 mice. Metabolomics study showed BE restored the TCA cycle in plasma. Metabolic profiling of the respective brain parts suggested BE was able to regulate mitochondria activity, oxidative stress, fatty acid metabolism, neuroinflammation, neurotransmission, and amino acid homeostasis in the brains of AD mice via starch and sucrose metabolism, and glycolipid metabolism in cortex and hippocampus. Therefore, chronic treatment with BE could be a promising treatment strategy for AD.

Funding

The behavioural experiments were carried out at the Neuroscience Phenotyping Core Facility, which is supported by the National Medical Research Council/National University Health System (NMRC NUHS) Centre Grant - Neuroscience Phenotyping Core (NMRC/CG/M009/2017_NUH/NUHS). This work was supported by the National University of Singapore Academic Research Fund [grant number R148-000-064-012].

Author contributions

P.C.H, L.Z., and L.H. conceived and designed the experiments; Y.L. provided and tested the genotype of mice; P.W. performed the animal behavioural tests; W.X.S. performed the molecular docking estimation; L.Z., L.R.W, S.Y., and L.H. performed the rest of the experiments; P.C.H, L.Z. and L.R.W. were involved in the analysis and interpretation of the data; P.C.H, and L.Z. wrote and edited the work.

Data statement

Anonymized data will be shared by request from any qualified investigator.

Declaration of competing interest

The authors report no competing interest.

Data availability

Data will be made available on request.

Acknowledgements

We are grateful to Professor G. S. Dawe, Department of Pharmacology, National University of Singapore (Singapore) for kindly providing the animal source.

Appendix A. Supplementary data

Supplementary data to this article can be found online at https://doi.org/10.1016/j.bbih.2023.100599.

References

Aghajanzadeh, M., Andalib, S., Danafar, H., Rostamizadeh, K., Sharafi, A., 2020. The effect of baicalein-loaded Y-shaped miktoarm copolymer on spatial memory and hippocampal expression of DHCR24, SELADIN and SIRT6 genes in rat model of Alzheimer. Int. J. Pharm. 586, 119546 https://doi.org/10.1016/j.ijpharm.2020.119546.

Badhwar, A., Brown, R., Stanimirovic, D.B., Haqqani, A.S., Hamel, E., 2017. Proteomic differences in brain vessels of Alzheimer's disease mice: normalization by PPARgamma agonist pioglitazone. J. Cerebr. Blood Flow Metabol. 37, 1120–1136. https://doi.org/10.1177/0271678X16655172.

Craig, L.A., Hong, N.S., McDonald, R.J., 2011. Revisiting the cholinergic hypothesis in the development of Alzheimer's disease. Neurosci. Biobehav. Rev. 35, 1397–1409. https://doi.org/10.1016/j.neubiorev.2011.03.001.

de Jong, D.L.K., de Heus, R.A.A., Rijpma, A., Donders, R., Olde Rikkert, M.G.M., Gunther, M., Lawlor, B.A., van Osch, M.J.P., Jahr, Claassen, 2019. Effects of nilvadipine on cerebral blood flow in patients with alzheimer disease. Hypertension 74, 413–420. https://doi.org/10.1161/HYPERTENSIONAHA.119.12892.

Gong, Y., Liu, Y., Zhou, L., Di, X., Li, W., Li, Q., Bi, K., 2015. A UHPLC-TOF/MS method based metabonomic study of total ginsenosides effects on Alzheimer disease mouse model. J. Pharm. Biomed. Anal. 115, 174–182. https://doi.org/10.1016/j.jpba.2015.07.007.

Gonzales, C., Zaleska, M.M., Riddell, D.R., Atchison, K.P., Robshaw, A., Zhou, H., Sukoff Rizzo, S.J., 2014. Alternative method of oral administration by peanut butter pellet formulation results in target engagement of BACE1 and attenuation of gavage-induced stress responses in mice. Pharmacol. Biochem. Behav. 126, 28–35. https://doi.org/10.1016/j.pbb.2014.08.010.

Gonzalez-Dominguez, R., Garcia-Barrera, T., Gomez-Ariza, J.L., 2014a. Combination of metabolomic and phospholipid-profiling approaches for the study of Alzheimer's disease. J. Proteonomics 104, 37–47. https://doi.org/10.1016/j.jprot.2014.01.014.

Gonzalez-Dominguez, R., Garcia-Barrera, T., Gomez-Ariza, J.L., 2015a. Metabolite profiling for the identification of altered metabolic pathways in Alzheimer's disease. J. Pharm. Biomed. Anal. 107, 75–81. https://doi.org/10.1016/j.jpba.2014.10.010.

Gonzalez-Dominguez, R., Garcia-Barrera, T., Vitorica, J., Gomez-Ariza, J.L., 2014b. Region-specific metabolic alterations in the brain of the APP/PS1 transgenic mice of Alzheimer's disease. Biochim. Biophys. Acta 1842, 2395–2402. https://doi.org/10.1016/j.bbadis.2014.09.014.

Gonzalez-Dominguez, R., Garcia-Barrera, T., Vitorica, J., Gomez-Ariza, J.L., 2015b. Application of metabolomics based on direct mass spectrometry analysis for the elucidation of altered metabolic pathways in serum from the APP/PS1 transgenic model of Alzheimer's disease. J. Pharm. Biomed. Anal. 107, 378–385. https://doi.org/10.1016/j.jpba.2015.01.025.

Gonzalez-Dominguez, R., Garcia-Barrera, T., Vitorica, J., Gomez-Ariza, J.L., 2015c. Deciphering metabolic abnormalities associated with Alzheimer's disease in the APP/PS1 mouse model using integrated metabolomic approaches. Biochimie 110, 119–128. https://doi.org/10.1016/j.biochi.2015.01.005.

Gonzalez-Dominguez, R., Garcia-Barrera, T., Vitorica, J., Gomez-Ariza, J.L., 2015d. Metabolomic screening of regional brain alterations in the APP/PS1 transgenic model of Alzheimer's disease by direct infusion mass spectrometry. J. Pharm. Biomed. Anal. 102, 425–435. https://doi.org/10.1016/j.jpba.2014.10.009.

Gonzalez-Dominguez, R., Garcia-Barrera, T., Vitorica, J., Gomez-Ariza, J.L., 2015e. Metabolomics reveals significant impairments in the immune system of the APP/PS1 transgenic mice of Alzheimer's disease. Electrophoresis 36, 577–587. https://doi.org/10.1002/elps.201400450.

Griffiths, W.J., Koal, T., Wang, Y., Kohl, M., Enot, D.P., Deigner, H.P., 2010. Targeted metabolomics for biomarker discovery. Angew Chem. Int. Ed. Engl. 49, 5426–5445. https://doi.org/10.1002/anie.200905579.

Guo, L., Tian, J., Du, H., 2017. Mitochondrial dysfunction and synaptic transmission failure in alzheimer's disease. J Alzheimers Dis 57, 1071–1086. https://doi.org/10.3233/JAD-160702.

He, X.L., Wang, Y.H., Gao, M., Li, X.X., Zhang, T.T., Du, G.H., 2009. Baicalein protects rat brain mitochondria against chronic cerebral hypoperfusion-induced oxidative damage. Brain Res. 1249, 212–221. https://doi.org/10.1016/j.brainres.2008.10.005.

Hecht, N., He, J., Kremenetskaia, I., Nieminen, M., Vajkoczy, P., Woitzik, J., 2012. Cerebral hemodynamic reserve and vascular remodeling in C57/BL6 mice are influenced by age. Stroke 43, 3052–3062. https://doi.org/10.1161/STROKEAHA.112.653204.

Hong, S., Beja-Glasser, V.F., Nfonoyim, B.M., Frouin, A., Li, S., Ramakrishnan, S., Merry, K.M., Shi, Q., Rosenthal, A., Barres, B.A., Lemere, C.A., Selkoe, D.J., Stevens, B., 2016. Complement and microglia mediate early synapse loss in

Alzheimer mouse models. Science 352, 712–716. https://doi.org/10.1126/science.aad8373.
Huang, Y., Tsang, S.Y., Yao, X., Chen, Z.Y., 2005. Biological properties of baicalein in cardiovascular system. Curr. Drug Targets - Cardiovasc. Hematol. Disord. 5, 177–184. https://doi.org/10.2174/1568006043586206.
Ibanez, C., Simo, C., Barupal, D.K., Fiehn, O., Kivipelto, M., Cedazo-Minguez, A., Cifuentes, A., 2013. A new metabolomic workflow for early detection of Alzheimer's disease. J. Chromatogr. A 1302, 65–71. https://doi.org/10.1016/j.chroma.2013.06.005.
Lalande, J., Halley, H., Balayssac, S., Gilard, V., Dejean, S., Martino, R., Frances, B., Lassalle, J.M., Malet-Martino, M., 2014. 1H NMR metabolomic signatures in five brain regions of the AbetaPPswe Tg2576 mouse model of Alzheimer's disease at four ages. J Alzheimers Dis 39, 121–143. https://doi.org/10.3233/JAD-130023.
Li, S., Li, J., Pan, R., Cheng, J., Cui, Q., Chen, J., Yuan, Z., 2021. Sodium rutin extends lifespan and health span in mice including positive impacts on liver health. Br. J. Pharmacol. https://doi.org/10.1111/bph.15410.
Li, W.H., Yang, Y.L., Cheng, X., Liu, M., Zhang, S.S., Wang, Y.H., Du, G.H., 2020. Baicalein attenuates caspase-independent cells death via inhibiting PARP-1 activation and AIF nuclear translocation in cerebral ischemia/reperfusion rats. Apoptosis 25, 354–369. https://doi.org/10.1007/s10495-020-01600-w.
Lin, A.L., Zheng, W., Halloran, J.J., Burbank, R.R., Hussong, S.A., Hart, M.J., Javors, M., Shih, Y.Y., Muir, E., Solano Fonseca, R., Strong, R., Richardson, A.G., Lechleiter, J. D., Fox, P.T., Galvan, V., 2013. Chronic rapamycin restores brain vascular integrity and function through NO synthase activation and improves memory in symptomatic mice modeling Alzheimer's disease. J. Cerebr. Blood Flow Metabol. 33, 1412–1421. https://doi.org/10.1038/jcbfm.2013.82.
Liu, M., Zhang, X., Li, B., Wang, B., Wu, Q., Shang, F., Li, A., Li, H., Xiu, R., 2018. Laser Doppler: a tool for measuring pancreatic islet microvascular vasomotion in vivo. JoVE. https://doi.org/10.3791/56028.
Liu, Q., Xi, Y., Wang, Q., Liu, J., Li, P., Meng, X., Liu, K., Chen, W., Liu, X., Liu, Z., 2021. Mannan oligosaccharide attenuates cognitive and behavioral disorders in the 5xFAD Alzheimer's disease mouse model via regulating the gut microbiota-brain axis. Brain Behav. Immun. 95, 330–343. https://doi.org/10.1016/j.bbi.2021.04.005.
Liu, Z., Jiang, M., Kang, T., Miao, D., Gu, G., Song, Q., Yao, L., Hu, Q., Tu, Y., Pang, Z., Chen, H., Jiang, X., Gao, X., Chen, J., 2013. Lactoferrin-modified PEG-co-PCL nanoparticles for enhanced brain delivery of NAP peptide following intranasal administration. Biomaterials 34, 3870–3881. https://doi.org/10.1016/j.biomaterials.2013.02.003.
Ma, J., Wang, C., Sun, Y., Pang, L., Zhu, S., Liu, Y., Zhu, L., Zhang, S., Wang, L., Du, L., 2020. Comparative study of oral and intranasal puerarin for prevention of brain injury induced by acute high-altitude hypoxia. Int. J. Pharm. 591 https://doi.org/10.1016/j.ijpharm.2020.120002.
Martins, R.N., Harper, C.G., Stokes, G.B., Masters, C.L., 1986. Increased cerebral glucose-6-phosphate dehydrogenase activity in Alzheimer's disease may reflect oxidative stress. J. Neurochem. 46, 1042–1045. https://doi.org/10.1111/j.1471-4159.1986.tb00615.x.
Martire, S., Mosca, L., d'Erme, M., 2015. PARP-1 involvement in neurodegeneration: a focus on Alzheimer's and Parkinson's diseases. Mech. Ageing Dev. 146–148, 53–64. https://doi.org/10.1016/j.mad.2015.04.001.
Oksanen, M., Lehtonen, S., Jaronen, M., Goldsteins, G., Hamalainen, R.H., Koistinaho, J., 2019. Astrocyte alterations in neurodegenerative pathologies and their modeling in human induced pluripotent stem cell platforms. Cell. Mol. Life Sci. 76, 2739–2760. https://doi.org/10.1007/s00018-019-03111-7.
Paglia, G., Stocchero, M., Cacciatore, S., Lai, S., Angel, P., Alam, M.T., Keller, M., Ralser, M., Astarita, G., 2016. Unbiased metabolomic investigation of Alzheimer's Disease brain points to dysregulation of mitochondrial aspartate metabolism. J. Proteome Res. 15, 608–618. https://doi.org/10.1021/acs.jproteome.5b01020.
Pena-Bautista, C., Roca, M., Hervas, D., Cuevas, A., Lopez-Cuevas, R., Vento, M., Baquero, M., Garcia-Blanco, A., Chafer-Pericas, C., 2019. Plasma metabolomics in early Alzheimer's disease patients diagnosed with amyloid biomarker. J. Proteonomics 200, 144–152. https://doi.org/10.1016/j.jprot.2019.04.008.
Peng, J., Guo, K., Xia, J., Zhou, J., Yang, J., Westaway, D., Wishart, D.S., Li, L., 2014. Development of isotope labeling liquid chromatography mass spectrometry for mouse urine metabolomics: quantitative metabolomic study of transgenic mice related to Alzheimer's disease. J. Proteome Res. 13, 4457–4469. https://doi.org/10.1021/pr500828v.
Poinsatte, K., Selvaraj, U.M., Ortega, S.B., Plautz, E.J., Kong, X., Gidday, J.M., Stowe, A. M., 2015. Quantification of neurovascular protection following repetitive hypoxic preconditioning and transient middle cerebral artery occlusion in mice. JoVE, e52675. https://doi.org/10.3791/52675.
Quartey, M.O., Nyarko, J.N.K., Pennington, P.R., Heistad, R.M., Chaharyn, B.M., Wei, Z., Bainbridge, D., Baker, G.B., Mousseau, D.D., 2019. Age- and sex-dependent profiles of APP fragments and key secretases align with changes in despair-like behavior and cognition in young APPSwe/Ind mice. Biochem. Biophys. Res. Commun. 511, 454–459. https://doi.org/10.1016/j.bbrc.2019.02.083.
Rajasekar, N., Nath, C., Hanif, K., Shukla, R., 2017. Intranasal insulin improves cerebral blood flow, Nrf-2 expression and BDNF in STZ (ICV)-induced memory impaired rats. Life Sci. 173, 1–10. https://doi.org/10.1016/j.lfs.2016.09.020.
Rong, W., Ding, K., Guo, S., Xie, F., Li, Q., Bi, K., 2019. Metabolomics analysis of Xanthoceras sorbifolia husks protection of rats against Alzheimer's disease using liquid chromatography mass spectrometry. J. Chromatogr., B: Anal. Technol. Biomed. Life Sci. 1126–1127 https://doi.org/10.1016/j.jchromb.2019.121739.
Saffari, P.M., Alijanpour, S., Takzaree, N., Sahebgharani, M., Etemad-Moghadam, S., Noorbakhsh, F., Partoazar, A., 2020. Metformin loaded phosphatidylserine nanoliposomes improve memory deficit and reduce neuroinflammation in streptozotocin-induced Alzheimer's disease model. Life Sci. 255 https://doi.org/10.1016/j.lfs.2020.117861.
Salek, R.M., Xia, J., Innes, A., Sweatman, B.C., Adalbert, R., Randle, S., McGowan, E., Emson, P.C., Griffin, J.L., 2010. A metabolomic study of the CRND8 transgenic mouse model of Alzheimer's disease. Neurochem. Int. 56, 937–947. https://doi.org/10.1016/j.neuint.2010.04.001.
Santos, A.L.M., Vitorio, J.G., de Paiva, M.J.N., Porto, B.L.S., Guimaraes, H.C., Canuto, G. A.B., Carvalho, M.D.G., de Souza, L.C., de Toledo, J.S., Caramelli, P., Duarte-Andrade, F.F., Gomes, K.B., 2020. Frontotemporal dementia: plasma metabolomic signature using gas chromatography-mass spectrometry. J. Pharm. Biomed. Anal. 189, 113424 https://doi.org/10.1016/j.jpba.2020.113424.
Sun, B., Zhou, Y., Halabisky, B., Lo, I., Cho, S.H., Mueller-Steiner, S., Devidze, N., Wang, X., Grubb, A., Gan, L., 2008. Cystatin C-cathepsin B axis regulates amyloid beta levels and associated neuronal deficits in an animal model of Alzheimer's disease. Neuron 60, 247–257. https://doi.org/10.1016/j.neuron.2008.10.001.
Thapa, K., Khan, H., Sharma, U., Grewal, A.K., Singh, T.G., 2021. Poly (ADP-ribose) polymerase-1 as a promising drug target for neurodegenerative diseases. Life Sci. 267, 118975 https://doi.org/10.1016/j.lfs.2020.118975.
Trushina, E., Dutta, T., Persson, X.M., Mielke, M.M., Petersen, R.C., 2013. Identification of altered metabolic pathways in plasma and CSF in mild cognitive impairment and Alzheimer's disease using metabolomics. PLoS One 8, e63644. https://doi.org/10.1371/journal.pone.0063644.
Trushina, E., Mielke, M.M., 2014. Recent advances in the application of metabolomics to Alzheimer's Disease. Biochim. Biophys. Acta 1842, 1232–1239. https://doi.org/10.1016/j.bbadis.2013.06.014.
Tsuruoka, M., Hara, J., Hirayama, A., Sugimoto, M., Soga, T., Shankle, W.R., Tomita, M., 2013. Capillary electrophoresis-mass spectrometry-based metabolome analysis of serum and saliva from neurodegenerative dementia patients. Electrophoresis 34, 2865–2872. https://doi.org/10.1002/elps.201300019.
Varshavi, D., Scott, F.H., Varshavi, D., Veeravalli, S., Phillips, I.R., Veselkov, K., Strittmatter, N., Takats, Z., Shephard, E.A., Everett, J.R., 2018. Metabolic biomarkers of ageing in C57bl/6J wild-type and flavin-containing monooxygenase 5 (FMO5)-Knockout mice. Front. Mol. Biosci. 5, 28. https://doi.org/10.3389/fmolb.2018.00028.
Verwaest, K.A., Vu, T.N., Laukens, K., Clemens, L.E., Nguyen, H.P., Van Gasse, B., Martins, J.C., Van Der Linden, A., Dommisse, R., 2011. (1)H NMR based metabolomics of CSF and blood serum: a metabolic profile for a transgenic rat model of Huntington disease. Biochim. Biophys. Acta 1812, 1371–1379. https://doi.org/10.1016/j.bbadis.2011.08.001.
Walker, J.M., Fowler, S.W., Miller, D.K., Sun, A.Y., Weisman, G.A., Wood, W.G., Sun, G. Y., Simonyi, A., Schachtman, T.R., 2011. Spatial learning and memory impairment and increased locomotion in a transgenic amyloid precursor protein mouse model of Alzheimer's disease. Behav. Brain Res. 222, 169–175. https://doi.org/10.1016/j.bbr.2011.03.049.
Wang, G., Zhou, Y., Huang, F.J., Tang, H.D., Xu, X.H., Liu, J.J., Wang, Y., Deng, Y.L., Ren, R.J., Xu, W., Ma, J.F., Zhang, Y.N., Zhao, A.H., Chen, S.D., Jia, W., 2014. Plasma metabolite profiles of Alzheimer's disease and mild cognitive impairment. J. Proteome Res. 13, 2649–2658. https://doi.org/10.1021/pr5000895.
Wei, D., Tang, J., Bai, W., Wang, Y., Zhang, Z., 2014. Ameliorative effects of baicalein on an amyloid-beta induced Alzheimer's disease rat model: a proteomics study. Curr. Alzheimer Res. 11, 869–881. https://doi.org/10.2174/1567205011666141001113619.
Wissmann, P., Geisler, S., Leblhuber, F., Fuchs, D., 2013. Immune activation in patients with Alzheimer's disease is associated with high serum phenylalanine concentrations. J. Neurol. Sci. 329, 29–33. https://doi.org/10.1016/j.jns.2013.03.007.
Wong, L.R., Tan, E.A., Lim, M.E.J., Shen, W., Lian, X.L., Wang, Y., Chen, L., Ho, P.C., 2021. Functional effects of berberine in modulating mitochondrial dysfunction and inflammatory response in the respective amyloidogenic cells and activated microglial cells - in vitro models simulating Alzheimer's disease pathology. Life Sci. 282, 119824 https://doi.org/10.1016/j.lfs.2021.119824.
Wong, L.R., Wong, P., Ho, P.C., 2020. Metabolic profiling of female Tg2576 mouse brains provides novel evidence supporting intranasal low-dose pioglitazone for long-Term treatment at an early stage of Alzheimer's disease. Biomedicines 8. https://doi.org/10.3390/biomedicines8120589.
Zhang, L., Li, M., Zhan, L., Lu, X., Liang, L., Su, B., Sui, H., Gao, Z., Li, Y., Liu, Y., Wu, B., Liu, Q., 2015. Plasma metabolomic profiling of patients with diabetes-associated cognitive decline. PLoS One 10, e0126952. https://doi.org/10.1371/journal.pone.0126952.
Zhang, L., Yang, S., Huang, L., Ho, P.C., 2020. Poly (ethylene glycol)-block-poly (D, L-lactide) (PEG-PLA) micelles for brain delivery of baicalein through nasal route for potential treatment of neurodegenerative diseases due to oxidative stress and inflammation: an in vitro and in vivo study. Int. J. Pharm. 591, 119981 https://doi.org/10.1016/j.ijpharm.2020.119981.
Zhang, N., Gordon, M.L., Goldberg, T.E., 2017. Cerebral blood flow measured by arterial spin labeling MRI at resting state in normal aging and Alzheimer's disease. Neurosci. Biobehav. Rev. 72, 168–175. https://doi.org/10.1016/j.neubiorev.2016.11.023.
Zhou, Y., Wei, M., Fan, M., Liu, Z., Wang, A., Liu, Y., Men, L., Pi, Z., Liu, Z., Song, F., 2021. Pharmacokinetic and metabolomics approach based on UHPLC-MS to evaluate therapeutic effect of lignans from S. Chinensis in alzheimer's disease. J. Chromatogr., B: Anal. Technol. Biomed. Life Sci. 1178, 122859 https://doi.org/10.1016/j.jchromb.2021.122859.